Electronic structure of $KTi(SO_4)_2 \cdot H_2O$ - a S=1/2 frustrated chain antiferromagnet

Deepa Kasinathan,[1,*] K. Koepernik,[2] O. Janson,[1] G. J. Nilsen,[3] J. O. Piatek,[3] H. M. Rønnow,[3] and H. Rosner[1,†]

[1] *Max Planck Institut für Chemische Physik fester Stoffe, Nöthnitzer Str. 40, 01187 Dresden, Germany*
[2] *IFW Dresden, P.O. Box 270116, D-01171 Dresden, Germany*
[3] *Laboratory for Quantum Magnetism, ICMP, EPFL, CH-1015, Lausanne, Switzerland*

(Dated: April 12, 2013)

The compound $KTi(SO_4)_2 \cdot H_2O$ was recently reported as a quasi one-dimensional spin 1/2 compound with competing antiferromagnetic nearest neighbor exchange J_1 and next-nearest neighbor exchange J_2 along the chain with a frustration ratio $\alpha = J_2/J_1 \approx 0.29$ [Chem. Mater. **20**, 8 (2008)]. Here, we report a microscopically based magnetic model for this compound derived from density functional electronic structure calculations along with respective tight-binding models. Our calculations confirm the quasi one-dimensional nature of the system with antiferromagnetic J_1 and J_2, but suggest a significantly larger frustration ratio $\alpha \approx 1.1 \pm 0.2$. Based on transfer matrix renormalization group calculations we found that, due to an intrinsic symmetry of the J_1-J_2 model, our larger frustration ratio α is also consistent with the previous thermodynamic data. To resolve this issue, we propose performing high-field magnetization measurements and low temperature susceptibility measurements which should allow to precisely identify the frustration ratio α.

PACS numbers: look it up

arXiv:1304.3361v1 [cond-mat.str-el] 11 Apr 2013

I. INTRODUCTION

For several decades, low dimensional magnetism has attracted great interest in solid state physics and chemistry. Since the influence of quantum fluctuations becomes especially pronounced for low dimensional spin-1/2 systems, these systems have been investigated extensively, both theoretically and experimentally. Quantum fluctuations become even more important in determining the ground state and the nature of the low lying excitations if the system under consideration exhibits strongly frustrated interactions.

Whereas pure geometrical frustration, i.e triangular, Kagomé or pyrochlore lattices, can be realized by special symmetries in two or more dimensions, frustration in one-dimensional systems (linear chains) is generally realized by competing interactions. The simplest frustrated one dimensional model is the J_1-J_2 model with nearest neighbor (NN) exchange J_1 and next nearest neighbor (NNN) exchange J_2, where J_2 is antiferromagnetic. The phase diagram of this seemingly simple model is very rich. Depending on the frustration ratio $\alpha = J_2/J_1$, a variety of ground states are observed in corresponding quasi-1D systems: (i) ferromagnetically ordered chains in Li_2CuO_2[1,2] ($0 \leq |\alpha| \leq 0.25$); (ii) helical order with different pitch angles in $LiVCuO_4$, $LiCu_2O_2$, and $NaCu_2O_2$[3–9] ($\alpha < -0.25$); (iii) spin-Peierls transition in $CuGeO_3$[10,11] ($\alpha \gtrsim 0.2411$), i.e. both exchange couplings are antiferromagnetic.

The possibility of subtle interplay between spin, orbital, charge and lattice degrees of freedom due to the threefold orbital degeneracy of Ti^{3+} in octahedral environments, makes titanium 3+ based oxides an interesting class of materials to study. Exotic features like orbital-liquid state in $LaTiO_3$ and presence of strong orbital fluctuations in $YTiO_3$ have been reported.[12,13] While an abundance of experimental work exists on low dimensional spin-1/2 cuprates (with Cu^{2+}), materials based on spin-1/2 titanates (with Ti^{3+}) are rather sparse. A well known example of low-dimensional titanates is the new class of inorganic spin-Peierls materials $TiOX$ (X = Cl, Br).[14] Quasi one-dimensional magnetism was observed in TiOCl and TiOBr along with a first-order transition to a dimerized non-magnetic ground state (spin-Peierls like) below 67 K and 27 K, respectively. The main difference between S=1/2 titanates and vanadates as compared to the cuprates ($3d^1$ vs. $3d^9$) is that the unpaired electron resides in the t_{2g} complex for the former, while occupying the e_g complex for the latter. This usually results in narrow bands at the Fermi level (E_F) for the titanates and vanadates as compared to the cuprates, which in turn leads to small values for the exchange couplings and brings several experimental conveniences. Since the temperature scale for the magnetic contribution to the specific heat is of the order of J, separating magnetic and phonon contribution in the specific heat (C_p) measurements is thus relatively easy. For the same reason, magnetization measurements can reach the saturation moment in experimentally attainable fields, thereby providing more information about the exchange parameters and the frustration regime. Thus, in many respects, spin 1/2 compounds with a singly occupied t_{2g} orbital are an ideal object to study the physics of quasi one-dimensional frustrated chains.

$KTi(SO_4)_4 \cdot H_2O$, a new member in the family of titanium alums has recently been synthesized[15]. The titanium ions are in the 3+ (d^1) oxidation state in this material. Specific heat and susceptibility measurements indicate that $KTi(SO_4)_4 \cdot H_2O$ is a S=1/2 frustrated chain system. Fits to the susceptibility data using exact diagonalization on up to 18 spins resulted in estimates for leading exchanges $J_1 = 9.46$ K and $J_2 = 2.8$ K, both AFM with $\alpha = 0.29$. In the well studied J_1-J_2 frustrated chain model with both interactions being AFM, the model un-

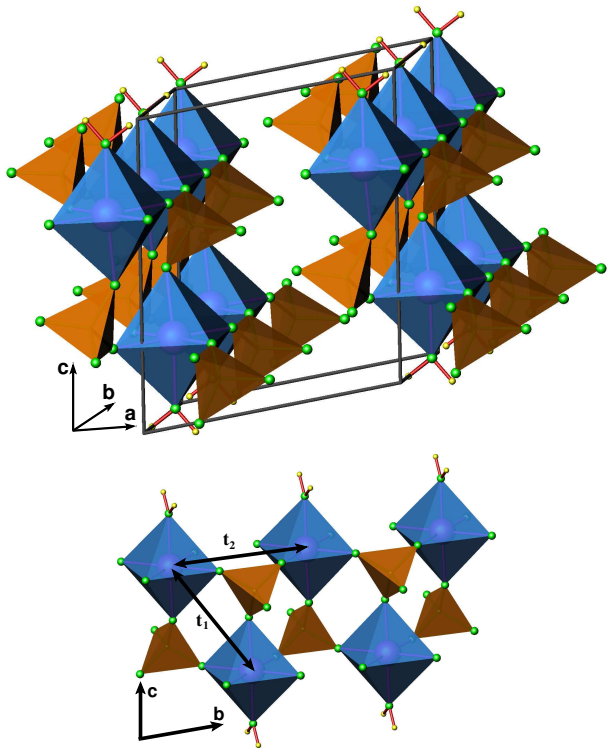

FIG. 1. (Color Online) **Top:** Crystal structure of $KTi(SO_4)_2{\cdot}H_2O$. Double chains of TiO_6 octahedra run along the b-axis. The octahedra are connected on either sides by SO_4 tetrahedra. Water molecules are bound to the octahedra and separating the double chains along the c-axis. The potassium atoms (not shown here) separate the double chains along the a-axis. **Bottom:** An isolated segment of the double chain. The nearest neighbor (NN) and next nearest neighbor (NNN) hopping paths are represented as t_1 and t_2 respectively.

dergoes a quantum phase transition at $\alpha = 0.2411$ to a two-fold degenerate gapped phase, and for $\alpha > 0.2411$ the system will exhibit spontaneous dimerization.[16–22] In light of this result, $KTi(SO_4)_4{\cdot}H_2O$ would be expected to occupy the highly interesting region of the phase diagram, with a small gap $\Delta < J_1/20$.[15,22]

Here, we report the results of an electronic structure analysis from first principles, carried out to obtain a microscopic picture of the origin of the low dimensional magnetism in $KTi(SO_4)_4{\cdot}H_2O$. The magnetically active orbital is identified using band structure calculations followed by subsequent analysis of the exchange couplings. The calculated J's have the same sign as the experiments (*i.e.* AFM), but the estimated frustration ratio α is considerably larger compared to the experimental findings. We explore in detail the reasons for this discrepancy and propose an alternative solution that fits the experimental data, as well as being consistent with our band structure calculations. To this end, we have simulated the temperature dependence of magnetic susceptibility using the transfer-matrix renormalization group (TMRG) method to unambiguously identify the exchange couplings that describe the microscopic magnetic model for $KTi(SO_4)_2{\cdot}H_2O$. On the basis of these results, we suggest performing high-field magnetization measurements, which will be a decisive experiment to identify the precise frustration ratio α. The influence of crystal water on the observed ground state is also discussed in detail.

The remainder of the manuscript is organized as follows: The crystal structure of $KTi(SO_4)_2{\cdot}H_2O$ is described in section II. The details of the various calculational methods are collected in section III. The results of the density functional theory based calculations, including the band structure and the accordingly derived microscopic model is described in section IV. In section V we demonstrate the effects of the crystal water in this compound by calculating the Wannier functions. The outcome of the TMRG simulations is compared to the previous experiment in section VI, which is followed by a discussion and summary in section VII.

II. CRYSTAL STRUCTURE

Throughout our calculations, we have used the recently determined experimental[15] lattice parameters in the monoclinic space group ($P2_1/m$) of $KTi(SO_4)_2{\cdot}H_2O$: $a = 7.649$ Å, $b = 5.258$ Å, $c = 9.049$ Å and $\beta = 101.742^\circ$. The crystal structure which is isomorphous to that of the mineral Krausite[23], $KFe(SO_4)_2{\cdot}H_2O$ is displayed in Fig. 1. Isolated pairs of chains ("double chains") of TiO_6 octahedra run along the crystallographic b-axis. The octahedra are distorted and have no edge sharing or corner sharing oxygen atoms. The SO_4 tetrahedra corner share with three adjacent TiO_6 octahedra, forming an isosceles triangle. These trangles edge-share to make up the double chains. The single chains are displaced with respect to each other both laterally and vertically. Large K^+ ions isolate the double chains along a, while along c the chains are separated by water molecules that share the oxygen atom with the TiO_6 octahedra. The water molecules are oriented in the ac plane. All of the octahedral O-Ti-O bond angles deviate slightly away from 90° and there are three pairs of Ti-O bond lengths of 2.001 Å, 2.056 Å (in the ab plane) and 2.043 Å (along c). The shortest Ti-Ti distance is 4.93 Å, and is between nearest neighbors (NN) on the adjacent chains (t_1 in Fig. 1). Within the chains, neighboring Ti are 5.23 Å apart(t_2 in Fig. 1). By analogy with the $J_1 - J_2$ Heisenberg model, we will call the magnetic interactions corresponding to the shorter distance (NN) J_1 and the longer distance (next nearest neighbors, NNN) J_2. In case of a perfect octahedral environment, the three t_{2g} states would be degenerate and thus warrant additional effects (*i.e.* lattice distortion, spin/charge/orbital ordering) to lift the degeneracy and allow for an S=1/2 singlet ground state for a Ti^{3+} ion.[24] In $KTi(SO_4)_2{\cdot}H_2O$, there is a small distortion of the octahedra and consequently splitting of the t_{2g} levels can be expected. The related case of Ti-

OCl, another system containing Ti^{3+} ion, also possesses a distorted arrangement of $TiCl_2O_4$ octahedra, though the distortions are much larger with equatorial Ti-O and Ti-Cl bond lengths of 2.25 Å and 2.32 Å, respectively, and an apical Ti-O bond length of 1.95 Å. Consequently, the t_{2g} orbitals in TiOCl were thought to split into a lower energy d_{xy} and higher energy $d_{xz,yz}$ orbitals. Electronic structure calculations confirmed this interpretation and revealed the magnetically active orbital for the S=1/2 chains in TiOCl was indeed the lower energy d_{xy} orbital,[14,25] though a prolonged discussion of possible orbital fluctuations ensued afterwards. Therefore, an analysis of $KTi(SO_4)_2{\cdot}H_2O$ from the structural point of view alone is not sufficient to determine the ground state of the system. Detailed calculations are necessary to understand the correct orbital and magnetic ground state of the system.

III. CALCULATIONAL DETAILS

The DFT calculations were performed using a full potential nonorthogonal local orbital code (FPLO) within the local (spin) density approximation (L(S)DA)[26,27]. The energies were converged on a dense k mesh with 300 points for the conventional cell in the irreducible wedge of the Brillouin zone. The Perdew and Wang flavor[28]of the exchange correlation potential was chosen for the scalar relativistic calculations. The strong on-site Coulomb repulsion of the Ti 3d orbital was taken into account using the L(S)DA+U method, applying the "atomic limit" double counting term. The projector on the correlated orbitals was defined such that the trace of the occupation number matrices represent the 3d gross occupation. The AFM parts of the exchange couplings are computed as $J_i^{\rm AFM} = 4t_i^2/U_{\rm eff}$, by mapping the results of the LDA calculations on to a tight binding model (TBM) which is then mapped on to a Hubbard model, and subsequently to a Heisenberg model because the system belongs to the strong correlation limit $U_{\rm eff} \gg t$ (t is the leading transfer integral at half filling). The full exchange couplings are obtained by mapping the LSDA+U_d total energies of various supercells with collinear spin configurations to a classical Heisenberg model. The supercells used to calculate J_1 and J_2 were sampled using 300 and 100 k points, respectively. Maximally localized Wannier functions (WF) were calculated for the Ti t_{2g} orbitals, also using FPLO[29], to obtain a visual insight of the relevant orbitals and superexchange paths.

The magnetic excitation spectrum of frustrated spin chains was simulated using exact diagonalization code from the ALPS package.[30] We used periodic boundary conditions and considered finite lattices comprising up to $N = 32$ spins.

The magnetic susceptibility of infinite frustrated spin chains was simulated using the transfer-matrix renormalization group (TMRG) technique.[31] For each simulation, we kept 120–160 states, the starting inverse temperature

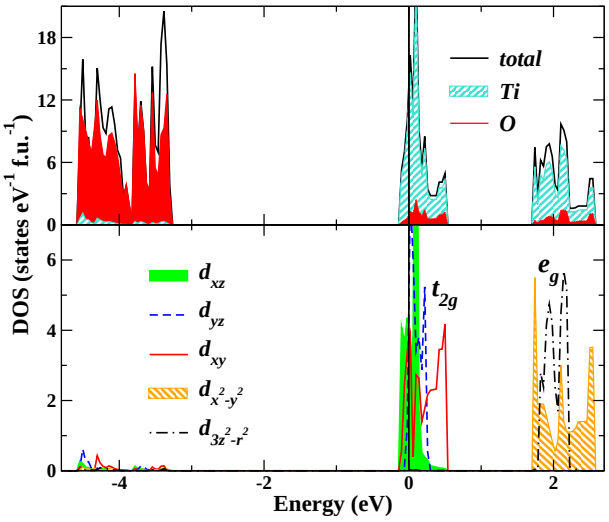

FIG. 2. (Color Online) Top: Total and partial DOS obtained within LDA for $KTi(SO_4)_2{\cdot}H_2O$. The valence panel is predominantly comprised of Ti-3d and O-2p states. The sulphur states (not shown here) lie mainly below -8 eV. The contribution from K, S and H sites are negligible in the displayed energy range. Bottom: Ti 3d-orbital resolved DOS. The t_{2g} and e_g complexes are split by a ligand field splitting of about 2 eV. The d_{xz} orbital and the d_{yz} orbital are very close and split from the broad d_{xy} (larger bandwidth) orbital.

was set to $0.05J_1$, and the Trotter number was varied between $4{\cdot}10^3$ and $16{\cdot}10^3$. The results were well converged for the whole temperature range of the experimental curve from Ref. 15.

IV. ELECTRONIC STRUCTURE CALCULATIONS

A. Local Density Approximation

Since there exists no previous report on the electronic structure of $KTi(SO_4)_2{\cdot}H_2O$, we begin by analyzing the results from a non-magentic LDA calculation. In a simplified, fully ionic model each Ti^{3+} ion is surrounded by a slightly distorted octahedron of O^{2-} ions. The pseudo octahedral coordination dictates a set of local axes for the conventional e_g and t_{2g} orbitals. The local coordinate system is chosen as $\hat{z} \parallel c$, and $\hat{x}$ and $\hat{y}$ axes are rotated by 45° around c with respect to the original a and b axes. The non-magnetic total and orbital resolved density of states (DOS) are collected in Fig. 2. The presented part of the valence band is predominantly comprised of Ti 3d and O 2p states belonging to TiO_6 octahedra. The states belonging to sulfur (not shown) lie below -8 eV and are therefore well separated from the TiO_6 states. The weight close to the Fermi level (E_F) is mainly from the Ti t_{2g} states which contain two electrons (one for each Ti in the unit cell) and are separated by a

ligand field splitting of about 2 eV from the higher lying (empty) e_g states. For an octahedral arrangement of oxygen anions around a $3d$ transition metal cation, a 2 eV ligand field split is rather typical. For $KTi(SO_4)_2{\cdot}H_2O$, the band width of the t_{2g} band complex is only 0.65 eV, about one third of the value for TiOCl ($\sim$2 eV)[25]. This difference arises from the fact that in TiOCl, the basic octahedral structural units $TiCl_2O_4$ are arranged such that they are corner-sharing in the a-direction and edge-sharing along the b-direction, leading to a larger interaction between the octahedral units and hence a larger t_{2g} band width. In contrast, the TiO_6 octahedral units in $KTi(SO_4)_2{\cdot}H_2O$ are neither corner- nor edge-sharing and hence the smaller t_{2g} band width.

The degeneracy between the t_{2g} orbitals is lifted due to the monoclinic symmetry of the crystal structure as seen in the non-magnetic band structure (Fig. 3). There are 2 Ti atoms per formula unit and therefore 6 t_{2g} bands close to E_F. The bands are highly dispersive along Γ-Y, X-M and XZ-MZ directions, which are along the crystallographic y-axis and remain rather flat along the other high symmetry directions. This implies that the main interaction between the Ti^{3+} ions is along the "double chain", while sizably smaller interactions are expected between the adjacent double chains. The band belonging to the d_{xz} orbital is lower in energy as compared to the d_{yz} and d_{xz} (nearly empty and larger band width) orbitals (also see Fig. 2). The mixing between the Ti $3d$ and the O $2p$ states close to E_F is less than 10% and similar to other systems where Ti occurs in the d^1 configuration. This scenario is different from the cuprates (d^9) where 30% of the contribution to the states at E_F stems from O $2p$. This fundamental difference in the strength of the hybridization between the transition metal ions and the oxygen ligands comes from the relative energies (Δ) of the oxygen p and the transition metal d bands. In cuprates, the highest (half-filled) $d_{x^2-y^2}$ orbital and the uppermost (filled) oxygen p-orbitals are rather close in energy ($\Delta \sim 2$ eV) resulting in a strong pd hybridization. In titanates, on the contrary, the t_{2g} orbitals lie much higher in energy than the uppermost (filled) oxygen p-orbitals ($\Delta \geq 3$ eV) and therefore exhibit significantly less pd hybridization. Upon hole doping, the holes would formally appear in the oxygen p-orbitals for cuprates and in one of the t_{2g} orbitals for titanates, characterizing them as charge-transfer and Mott-Hubbard systems, respectively.

Experimentally, $KTi(SO_4)_2{\cdot}H_2O$ is an insulator, but a metallic solution is obtained within LDA. Such metallic results from LDA are well known and understood to arise from the inadequate treatment of the strong Coulomb correlation of the $3d$ orbitals. Therefore, the orbital dependence of the Coulomb and exchange interactions are taken into account in a mean field like approximation using the LSDA+U approach (Section IV-C). As mentioned previously in Sec. II, the distorted octahedra in TiOCl split the t_{2g} states into a lower lying singlet (d_{xy}) and a higher energy doublet ($d_{xz,yz}$). Presuming no further symmetry breaking, adding correlations, the choice of the orbital for occupying the one unpaired electron of the Ti^{3+} ion in TiOCl is rather straightforward: the singlet d_{xy}. On the other hand, for $KTi(SO_4)_2{\cdot}H_2O$ the pseudo octahedral ligand field splits the t_{2g} states and removes the three fold degeneracy. Nevertheless, due to the relatively small energy differences, there is no clear candidate for the choice of the half-filled orbital. The band center of the d_{xz} orbital is around E_F and is the lowest lying band of the t_{2g} complex. The center of gravity of d_{yz} and the comparably broad d_{xy} band are only slightly higher in energy than the d_{xz} at 0.15 eV and 0.25 eV, respectively. Since the three t_{2g} orbitals are quite close in energy, a subtle balance between the orbitals is expected and therefore one should carefully consider the possibility of an orbitally ordered solution. At this juncture, it is rather unclear which correlated orbital will be half filled and thereby determine the magnetic model. Even the undoped, low dimensional S=1/2 cuprates that possess an extensive literature, where the magnetic model is generally understood to be governed by the half-filled $d_{x^2-y^2}$ orbital, can sometimes show surprises. For example, the CuO_6 octahedral environment in the insulating S=1/2 quasi 1D system $CuSb_2O_6$ is less distorted than usual, so that the cubic degeneracy for the e_g ligand-field states are only slightly lifted. The energy difference between the $d_{x^2-y^2}$ and $d_{3z^2-r^2}$ related band centers is about 0.3 eV only, compared with about 2 eV for standard cuprates. Inclusion of correlations, changes the order and results in the unpaired electron occupying the $d_{3z^2-r^2}$ orbital instead of the standard $d_{x^2-y^2}$ in $CuSb_2O_6$.[32]

We take into account the strong electronic correlations of the Ti $3d$ states via two possible ways: (a) mapping the results from LDA first to a tight-binding model (TBM), which in turn is mapped onto a Hubbard model,

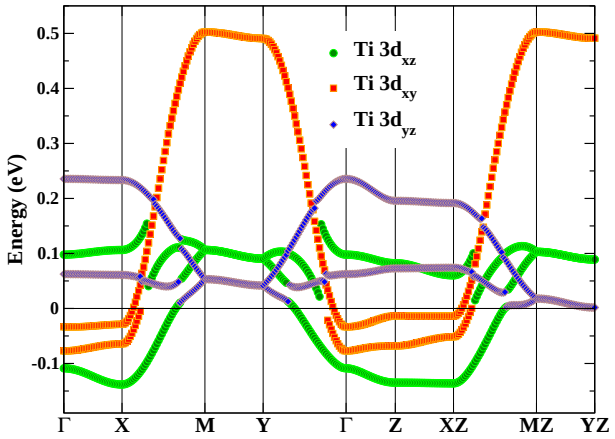

FIG. 3. (Color Online) Band structures with band character close to the Fermi level obtained within LDA. The bands are dispersive along Γ-Y and X-M direction - the crystallographic y direction along which the "double chains" propagate. There are two Ti atoms in the unit cell and therefore 6 t_{2g} bands crossing the Fermi energy.

	t_1 (eV)	t_2 (eV)	$J_1^{\rm AFM}$ (K)	$J_2^{\rm AFM}$ (K)	α
d_{xz}	0.047	0.029	31	11.8	0.38
d_{yz}	0.037	0.028	19	11	0.57
d_{xy}	0.081	0.135	92	256	2.78

TABLE I. Hopping parameters (in meV) and the corresponding exchange constants (in K) from an effective one-band TBM. The hopping paths are indicated in the lower panel of Fig. 1. The transfer integral t_1 corresponds to hopping between the single chanis, while t_2 corresponds to hopping within a single chain. A $U_{\rm eff}$ of 3.3 eV has been used to calculate the J's. The frustration ratio $\alpha = J_2/J_1$ is collected in the last column.

and subsequently to a Heisenberg model. At half filling, when U is much larger than the bandwidth w, the spin degrees of freedom are well described by an S=1/2 AFM Heisenberg Hamiltonian with an exchange interaction $J_i^{\rm AFM} \simeq 4t_i^2/U_{\rm eff}$. (b) performing LSDA+$U_d$ total energy calculations for various collinear spin configurations and mapping the energy differences on to a classical Heisenberg model to obtain the total exchange J. At this juncture, the difference between the two parameters used to incorporate the effects of strong correlations, $U_{\rm eff}$ and U_d must be clarified. The former is applied to LDA bands which include the effects of hybridization between the metal atoms and ligands, while the latter is applied to purely atomic d-orbitals and therefore necessitates using different values for these two parameters.

B. Tight Binding Model

Though LDA fails in reproducing the insulating ground state of $KTi(SO_4)_2{\cdot}H_2O$ system, it still provides valuable information about the orbitals involved in the low energy physics, as well as their corresponding interactions strengths. As mentioned previously, the strong Coulomb correlations favor full polarization and a detailed analysis is necessary to identify the ground state for the fully polarized d-orbital. Therefore, to obtain a microscopic picture of the magnetic interactions, we have first derived an effective one-band TBM for each set of the t_{2g} bands. For each set of the different "active" t_{2g} orbitals, we fit the corresponding LDA bands to a separate TBM. In second quantization formalism, the tight-binding Hamiltonian can be expressed as,

$$\hat{H}_{\rm TB} = \sum_{\langle i,j\rangle,\sigma} t_{ij}(\hat{c}^\dagger_{i\sigma}\hat{c}_{j\sigma} + \hat{c}^\dagger_{j\sigma}\hat{c}_{i\sigma}) + \sum_{i,\sigma}\epsilon_i\hat{c}^\dagger_{i\sigma}\hat{c}_{i\sigma} \qquad (1)$$

where $c^\dagger_{i\sigma}, c_{j\sigma}$ are the usual creation and annihilation operators; σ denotes the spin polarization; ϵ_i are the constant energy shifts with respect to the Fermi level; t_{ij} are the transfer integrals and $\langle i,j\rangle$ are the site indices.

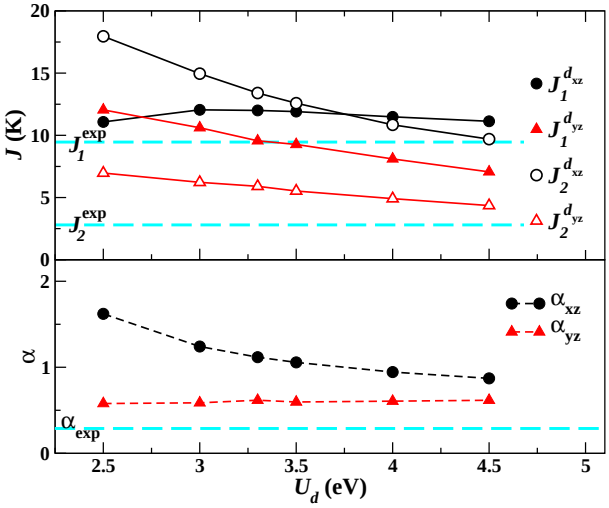

FIG. 4. (Color Online) The total exchange constants J's (top panel) and the frustration ratio α (bottom panel) as a function of U_d for d_{xz} and d_{yz} orbitals. The NN total exchange J_1 (full symbols) and NNN total exchange J_2 (empty symbols) do not vary much for the considered range of U_d (2.5 eV to 4.5 eV) values. The experimental results (Ref. 15) are indicated by dashed lines.

The magnitudes of the leading hopping integrals (the paths are indicated in Fig. 1) are collected in Table I. The NN (between single chains) and NNN (along the single chains) hopping integrals t_1 and t_2 are of the same order of magnitude for the d_{xz} and d_{yz} orbitals. On the contrary, the TBM fit to the broad d_{xy} orbital leads to a much larger t_2. All other t's beyond NNN are less than 0.1 meV for all the three orbitals and can be neglected for the chain physics. The two main hopping terms are thus confined to interactions between the Ti sites within each S = 1/2 "double chain", consistent with the experimental observations[15] of displaying low dimensional magnetic properties. The individual exchange constants are then calculated using $J_i^{\rm AFM} = 4t_i^2/U_{\rm eff}$. For TiOCl, a $U_{\rm eff} \sim 3.3$ eV was shown to provide good agreement between calculated exchange constants and susceptibility measurements[25]. The same value of $U_{\rm eff} = 3.3$ eV has been used here for $KTi(SO_4)_2{\cdot}H_2O$, the J's obtained are collected in Table. I. The J's for the lower energy d_{xz} band and as well as the d_{yz} band are of similar magnitude as compared to the experimental report. To the contrary, both the calculated NN and NNN J's for the d_{xy} band are much larger in energy compared to the experimental report. This large difference in the energy scale of the magnetic exchange for d_{xy} band implies that this orbital might be a rather unlikely choice for full polarization (a more clear picture emerges in the following section when performing LSDA+U calculations).

Since the constructed Heisenberg Hamiltonian takes into account only the antiferromagnetic component of the couplings, inclusion of ferromagnetic (FM) component could change the picture described above, especially

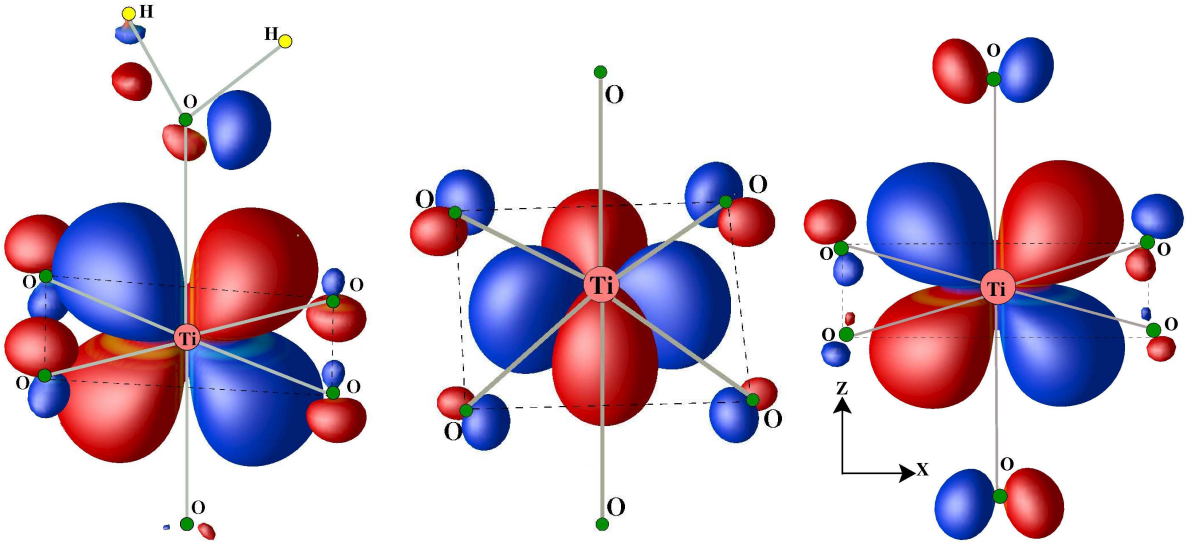

FIG. 5. (Color Online) Wannier functions of the three t_{2g} orbitals of the Ti^{3+} ion. **Left panel:** d_{xz}, **middle panel:** d_{xy}, **right panel:** d_{yz}. The blue and red lobes of the WF's refer to the positive and negative iso-surfaces, the circles refer to the atoms. The TiO_6 octahedra is highligted by the light grey Ti-O bonds. The perspective view is also aided by highlighting the crystallograhpic $a-b$ plane using dashed lines.

considering the absolute values for the AFM exchanges are quite small. In the proceeding section we report on the LSDA+U_d calculations to obtain the total exchange constants $J = J^{\rm FM} + J^{\rm AFM}$.

C. Density functional theory + U

Besides obtaining estimates for all the AFM couplings in the system, the TBM also allows for approximating the number of Ti-Ti neighbors that needs to be considered when performing the more involved and time consuming LSDA+U_d supercell calculations. Since the AFM exchanges obtained from the TBM beyond the NNN are less than 0.1 meV, and because FM interactions beyond second neighbors should also be small, we constructed two supercells to obtain the values of the short-ranged exchanges J_1 and J_2. Using different initial density matrices for the Ti $3d$ orbitals, one can correlate (fill the spin-up band with one electron and leave the spin-down band empty) the bands belonging to different irreducible representations. For $KTi(SO_4)_2{\cdot}H_2O$ we tried to spin-polarize each of the three t_{2g} bands. We considered U_d values ranging from 2.5 - 4.5 eV.[33] First let us consider the d_{xz} and d_{yz} orbitals, which gave similar AFM exchange constants in our TBM. In all of our LSDA+U_d calculations, the scenario in which the d_{xz} band was spin-polarized had the lowest energy. Spin-polarizing d_{yz} required an additional energy of 350 meV per Ti^{3+} ion. This energy scale is comparable to the band width of these orbitals. Incidentally, all our attempts to spin-polarize d_{xy} remained unsuccessful, though not unexpected when considering our TBM results (*i.e.* the much too large energy scale of J_2 which is inconsistent with experiments). We were also unable to stabilize different orbitally-ordered scenarios (*i.e.* one Ti ion with a spin-polarized d_{xz} orbital and the NN Ti ion with a spin-polarized d_{yz} orbital). This alludes to the fact that the (local) magnetic ground state in $KTi(SO_4)_2{\cdot}H_2O$ is very likely determined by the Ti $3d_{xz}$ orbital. The next question to answer is whether the exchange constants obtained for the d_{xz} orbital are consistent with the experimental findings. We obtain effective exchange constants by performing LSDA+U_d calculations of differently ordered spin configurations (FM, AFM and ferrimagnetic) and map the energies to a Heisenberg model. Among the considered spin configurations, the AFM spin configuration was always more favorable (lower total energy) than the FM. The exchange constants and the frustration ratio α are collected in Fig. 4. For comparison, we have displayed the values for both d_{xz} and d_{yz} orbitals. For the range of U_d values considered here, $J_1^{d_{xz}}$ is comparable to experimental findings while $J_2^{d_{xz}}$ is larger by almost an order of magnitude. Comparing the total J's in Fig. 4 with the $J^{\rm AFM}$ obtained from TBM in Table. I, we can infer that there is a significant FM component to the first neighbor ($J_1^{\rm FM}$) while the FM componet to the NNN ($J_2^{\rm FM}$) is quite negligible. Though the J's do not vary very much for U_d = 2.5 to 4.5 eV, an appropriate U_d value needs to be chosen for comparison with experiments. Spin- and orbital-unrestricted Hartree-Fock calculation of the on-site Coulomb interaction for various transition-metal oxides, recommend a U_d value of 4 eV for Ti^{3+} ions.[34] Using that value of U_d as a benchmark, we obtain, $J_1^{d_{xz}}$ $\approx$ 12 K, $J_2^{d_{xz}} \approx$ 13.4 K and $\alpha_{xz} \approx 0.94$ (J_1^{exp} = 9.46 K,

J_2^{exp} = 2.8 K, and α = 0.29). The calculated value of $\alpha_{xz} = J_2^{xz}/J_1^{xz}$ is larger than the experimental value by a factor of 4 for the d_{xz} orbital. The calculated α_{yz} (= 0.60) for the energetically unfavorable d_{yz} orbital is also somewhat larger than the experimental value. Albeit the S=1/2 frustrated chain magnetism in $KTi(SO_4)_2 \cdot H_2O$ is established in both LDA and LSDA+U_d calculations, our results for α are not consistent with the experiments. Nonetheless, both our calculation and experiment suggest an α in the highly interesting region ($0.2411 < \alpha <$ 1.8) of the spin-1/2 frustrated chain phase diagram.

In the following section, we attempt to understand the discrepancy between our calculations and the experiment.

V. EFFECT OF CRYSTAL WATER

A. Wannier Functions

The octahedron surrounding Ti^{3+} consists of 5 O^{2-} ions shared with SO_4^{2-} groups, and one water molecule (see Sec. II for a more detailed discussion). From a naive consideration of average equatorial and apical Ti-O distances, the magnetically active orbital would be assigned as d_{xy}. In contrast, both LDA and LSDA+U_d results point to d_{xz} as the magnetically active orbital. In order to shed some more light on this discrepancy, we have plotted the Wannier functions for the Ti t_{2g} complex (Fig. 5). Wannier functions are essentially a real-space picture of localized orbitals and can be used to enhance the understanding of bonding properties via an analysis of factors such as their shape and symmetry. Before analyzing the WF's, one should keep in mind that the two nearest neighbor (NN) Ti atoms do not belong to the same chain but to the pair-chain displaced along the c-axis (see lower panel of Fig. 1). By fitting (using exact diagonalization) the low temperature magnetic susceptibility, the recent experimental report[15] suggests that the AF-NN interaction J_1 is larger than the AF-NNN interaction J_2. Therefore, one expects to observe large tails at oxygen sites from the WF's bending towards the NN Ti atoms, as this facilitates the Ti-O-O-Ti superexchange. The Ti d_{xy} WF is composed of contributions from the d_{xy} orbital as well as tails on the oxygen sites in the xy-plane, although these do not point towards the NN Ti atom. The d_{yz} WF, on the otehr hand, has tails on all 6 oxygen sites of the TiO_6 octahedra, and all point towards the NN Ti atom. Interestingly, the d_{xz} WF not only has tails on the oxygen sites bending towards the NN Ti, but also has tails on one of the hydrogen site belonging to the crystal water molecule. Such an effect is arising from the hybridization effect of the O and H orbitals. The effects of hybridization involving the H-atom in the d_{yz} WF is comparatively less than the d_{xz}, since no extended tails are observed on the H site. We therefore infer that the orientation of the water molecule plays an important role in deciding the magnetically active orbital for obtaining the ground state in $KTi(SO_4)_2 \cdot H_2O$. More detailed analysis follows in the next section.

B. Rotating the water molecule

It is normally assumed that the presence of crystal water in a compound, leads to only modest changes in the crystal field of the magnetic ion. However, it might not always be the case. Recent work[35] on $CuCl_2$ and $CuCl_2 \cdot 2H_2O$ shows that the former is a quasi 1D-chain compound while the latter is a classical 3D AFM, although the magnetic Cu-Cl units in both compounds are structurally similar. Motivated by such reports and the results from our WF analysis, we explore the effects of the orientation of the H_2O molecule in $KTi(SO_4)_2 \cdot H_2O$. Crystallographic data that we have used until now orient the H_2O molecule in the xz plane. From the analysis of the WF's we infer that the magnetically active orbital (d_{xz}) is selected by the hydrogen bonding of the water molecule in the xz-plane with the Ti d_{xz} orbital. We now attempt to rotate the H_2O molecule to the yz plane and observe the effects on the electronic structure. The symmetry of the crystal was reduced to accommodate the new orientation, though the experimental O-H distance (0.8747 Å) as well as the H-O-H bond angle (93.33°) were left untouched. The resulting non-magnetic LDA band structure is displayed in Fig. 6. The general shape of the bands as well as the various k - point degeneracies are similar for both the xz and yz oriented H_2O molecule. The important changes for the fictitious yz oriented system are: (a) the d_{xz} band is no longer having the lowest band energy and is getting pushed upwards and therefore less occupied, (b) the d_{yz} band is pulled downwards and is getting more occupied. Ergo, the orientation of the H_2O molecule has a profound effect on the electronic structure and plays an important role in selecting the magnetically active orbital. In contrast with the LDA result, the addition of correlations results in d_{xz} as the lowest energy band, as was the case for H_2O —— xz. That said, the energy difference between singly occupied d_{xz} and d_{yz} is only 35 meV, 10 times smaller than the original calculation (cf. Sec. IV-C) in which the H_2O molecule was oriented along the xz-plane. Calculating the J's for the fictitious system using the effective TBM resulted in α_{yz} = 0.36 and a much larger α_{xz} = 1.11. These results reaffirm the the importance of the water molecule in deciding not only the magnetically active orbital, but also the accordingly derived exchanges and frustration ratio in $KTi(SO_4) \cdot H_2O$.

C. Effect of the O-H bond length

Having observed the sensitivity of the electronic structure to the orientation of the H_2O molecule, our next item of interest was to check the importance of the O-H bond length on the electronic structure and magnetic proper-

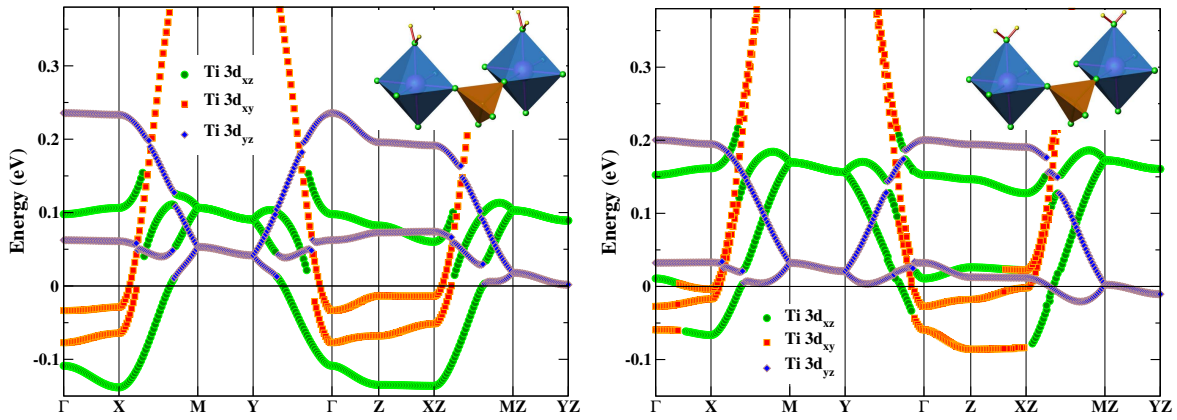

FIG. 6. (Color Online) Comparison of the non-magnetic band structure for $KTi(SO_4)_2{\cdot}H_2O$ using the reported xz-plane oriented (left) and the fictitious yz-plane oriented (right) H_2O molecule. The insets show a small segment of the double chains with the two respective orientations of the H_2O molecule.

ties. Recent reports on spin-1/2 kagome lattice systems[36] show a dramatic impact of the O-H bond length on the exchange. It is well known that obtaining the correct O-H bond length via X-ray diffraction in a system containing heavy atoms is difficult. OH^- impurity in oxides have been shown to have an equilibrium bond length of $\approx$ 1 Å.[37] For $KTi(SO_4)_2{\cdot}H_2O$, the reported O-H bond length is 10% smaller and only 0.874 Å. One possible reason for the larger frustration ratio α in LSDA+U_d calculations as compared to experiments might arise from the possibly underestimated O-H bond length.[38] We have therefore allowed the O-H bond length to relax. Keeping the TiO_6 octahedra rigid, we relaxed the H position with respect to the total energy and obtained an optimized O-H bond length of about 1 Å, in accordance with the empirical expectations.[36,37] Recalculating the exchange constants using the optimized O-H distance, we obtain for $U_d = 4.0$ eV, $J_1^{xz} = 10$ K, $J_2^{xz} = 14.2$ K. The frustration ratio $\alpha_{xz} = 1.4$ is even larger than the previously calculated value using the experimental O-H bond length. Thus far, all of our calculations have resulted in exchanges that have the correct sign and comparable magnitudes to the previous experimental report, but nonetheless always yielded frustration ratios far greater than previously reported.[15]. In the following section, we make a final attempt to clarify the discrepancy between the experiment and our calculations.

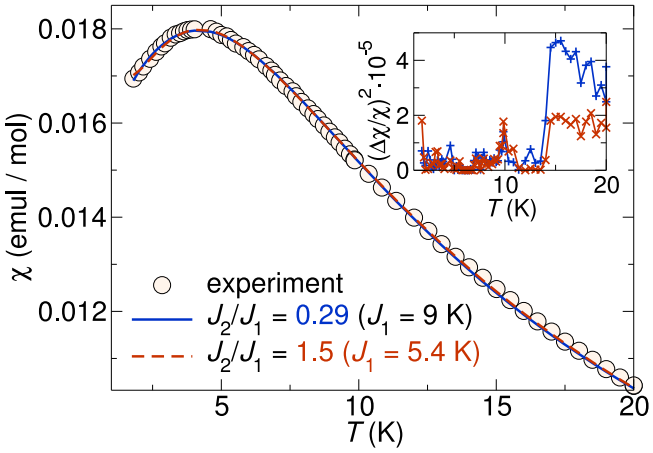

FIG. 7. (Color Online) Fits to the magnetic susceptibility. The experimental data are adopted from Ref. 15. Magnetic susceptibility of frustrated Heisenberg chains with $\alpha = 0.29$ and $\alpha = 1.5$ ($\alpha \equiv J_2/J_1$) was simulated using TMRG. The simulated curves were fitted to the experiment by varying the fitting parameters J_1, g and the temperature-independent contribution χ_0. Inset: difference curves for both solutions. $\Delta\chi$ is the difference between the simulated and the experimental value.

VI. TMRG CALCULATIONS

As demonstrated in Ref. 15, a frustrated Heisenberg chain model with $\alpha = 0.29$ can reproduce the experimental magnetic susceptibility curve of $KTi(SO_4)_2{\cdot}H_2O$. The small $\alpha = 0.29$ implies that J_1 is large, while J_2 is small. This is at odds with our LSDA+U_d calculations, where the antiferromagnetic exchange between NNN Ti atoms appears to be more efficient than the NN exchange. Thus, in the microscopic model, α should be larger than unity. The question is then, whether the large α regime conforms to the experimental behavior.

The small energy scale of the leading couplings leads to sizable error bars for the J_1 and J_2 values estimated from LSDA+U_d calculations. To refine the model parameters, we use the analytical expressions for the high-temperature part of the magnetic susceptibility of a frustrated Heisenberg chain, the high-temperature series expansion (HTSE).[39] Typical for a local optimization procedure, the results are dependent on the initial values. If we start from the $J_1 > J_2$ limit, HTSE yields $J_1 \simeq 9.6$

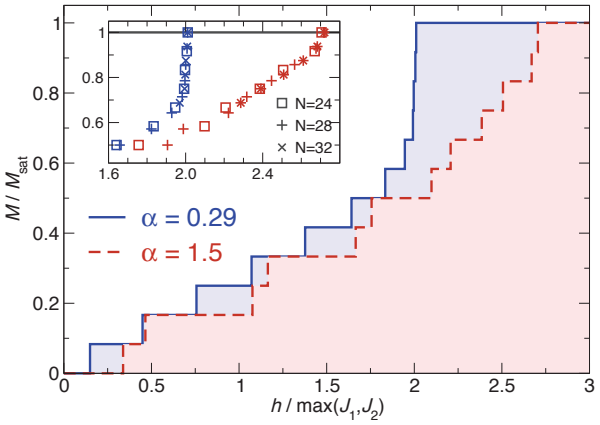

FIG. 8. (Color Online) Ground state magnetization of frustrated Heisenberg chains with $\alpha = 0.29$ and $\alpha = J_2/J_1 = 1.5$ ($\alpha \equiv J_2/J_1$), simulated using exact diagonalization on finite lattices (rings) of $N = 24$ spins. Note the characteristic upward bending of the $\alpha = 0.29$ curve. Inset: finite-size dependence of the ground state magnetization.

K and $J_2 \simeq 2.9$ K, very close to the $\alpha = 0.29$ reported in Ref. 15. In contrast, if we proceed from the $J_2 > J_1$ regime, we obtain $J_1 \simeq 5.4$ K and $J_2 \simeq 8.1$ K ($\alpha = 1.5$), in accord with our LSDA+U_d calculations. Thus, HTSE yields two ambiguous solutions.

HTSE typically diverges at temperatures comparable with the magnetic energy scale ($T \geq J$). To verify, whether both solutions agree with the experimental $\chi(T)$ at lower temperatures, we simulate the temperature dependence of reduced magnetic susceptibility $\chi*$ using TMRG, and fit the resulting $\chi^*(T/\max\{J_1, J_2\})$ dependencies to the experimental curve. In this way, we again find that besides the previously reported $\alpha = 0.29$ solution, the $\alpha = 1.5$ curve with $J_1 = 5.4$ K, $J_2 = 8.1$ K, $g = 1.74$, and $\chi_0 = 5.9{\cdot}10^{-5}$ emu/mol also yields an excellent fit to the experimental magnetic susceptibility (Fig. 7). The difference curves evidence that both $\alpha = 0.29$ and $\alpha = 1.5$ provide equally good description of the experimental $\chi(T)$ data (Fig. 7, inset).

The coexistence of the two solutions actually manifests the inner symmetry of the frustrated chain model. A trivial example: the uniform chain limit can be described with $\alpha = +0$ ($J_1 \neq 0$, $J_2 = 0$) as well as $\alpha = \infty$ ($J_1 = 0$, $J_2 \neq 0$). The $\alpha = 0.29$ and $\alpha = 1.5$ solutions are also related, although in a less trivial way. To pinpoint this relation, we revisit the phase diagram of the frustrated chain model. The $\alpha = 0$ limit corresponds to the exactly solvable gapless Heisenberg chain model. This GS is robust against small frustrating J_2, up to the quantum critical point $\alpha_c \simeq 0.2411$, where a spin gap opens.[40] For larger α values, the spin gap rapidly increases and reaches its maximum value $\Delta \simeq 0.43\,J_1$ at $\alpha \simeq 0.6$. Further enhancement of α reduces the spin gap. In the large α limit ($J_2 \gg J_1$), the spin gap exhibits an exponential decay.[41]

Thus, for a certain value of the spin gap Δ, there are two possible α values: (i) with a dominant J_1, i.e. from the $\alpha = 0.2411$–0.6 range, and (ii) with a sizable J_2 ($\alpha = 0.6$–∞). Since Δ plays a decisive role for the shape of $\chi(T)$, both solutions yield similar macroscopic magnetic behavior. This explains the seemingly unusual fact that the experimental data for $KTi(SO_4)_2{\cdot}H_2O$ can be fitted by both $\alpha = 0.29$ and $\alpha = 1.5$.

Despite the similar spin gaps, the solutions $\alpha = 0.29$ and $\alpha = 1.5$ are physically different (unlike, e.g. $\alpha = 0$ and $\alpha = \infty$, that describe the same physics): spiral correlations are present in the latter case, only.[41] Moreover, the two solutions feature substantially different correlation lengths.[41] Thus, the two solutions can be distinguished by measuring a characteristic experimental feature ("smoking gun").

For spin systems, a measurement of magnetization isotherms is technically simple, but very informative, especially for systems with weak magnetic couplings. Since the magnetic field linearly couples to the S^z component of the spin, a magnetization curve reflects the energy of the lowest lying state in each S^z sector. This often suffices to distinguish between ambiguous solutions. For instance, HTSE for the $J_1 - J_2$ square lattice system $BaCdVO(PO_4)_2$ yielded, besides the frustrated solution with an AFM J_2, also a nonfrustrated solution with AFM J_2. However, the frustrated scenario was clearly underpinned by $M(H)$ measurements.[42] In a recent work, $M(H)$ measurements for $A_2CuP_2O_7$ (A = Li,Na) resolved previous controversies concerning the magnetic dimensionality of these compounds.[43]

We argue that for the frustrated Heisenberg chain model, the characteristic behavior of magnetization on the verge of saturation can be used to distinguish between different scenarios. In particular, the $\alpha = 0.29$ magnetization curve exhibits a well pronounced upward bending, while only a feeble bending is visible in the $\alpha = 1.5$ GS magnetization (Fig. 8). Another relevant quantity is the saturation field:

$$H_{\rm sat} = (g\mu_{\rm B})^{-1}\left[E(S^z_{\rm max}) - E(S^z_{\rm max} - 1)\right], \qquad (2)$$

where $S^z_{\rm max}$ corresponds to the fully polarized state. The energies are estimated using exact diagonalization for finite chains of $N = 32$ spins. Adopting J_1, J_2, and g values from the HTSE fits, we obtain $H_{\rm sat} \simeq 16.4$ T and $H_{\rm sat} \simeq 18.7$ T for $\alpha = 0.29$ and $\alpha = 1.5$, respectively. Both values of saturation field lie in the experimentally accessible field range. A somewhat problematic point could be the low energy scale of $KTi(SO_4)_2{\cdot}H_2O$, which renders the typical measurement temperature of $\sim$1.5 K as relatively high, hence the states with different S^z could be substantially mixed. Still, the $\alpha = 0.29$ magnetization isotherms will retain fingerprints of the characteristic bending. Therefore, we believe that a high-field (up

to ∼20 T) measurement of a magnetization isotherm will be an instructive and decisive experiment to distinguish between the $\alpha = 0.29$ and $\alpha = 1.5$ scenarios.

VII. SUMMARY

In conclusion, we have studied the electronic structure of $KTi(SO_4)_2{\cdot}H_2O$ in detail using DFT based calculations. The results of both the TBM and LSDA+U_d calculations confirm beyond doubt the low dimensional nature of the material with NN and NNN exchanges J_1 and J_2 confined to the double-chains running along the b-axis. We also confirm the AFM nature of the exchanges, consistent with the experimental report, with the Ti-3d_{xz} orbital being the magnetically active one, holding the single unpaired electron of the Ti^{3+} ion. The magnitude of the calculated J's are of the right order compared to the experiment, though we observe a strong dependence to the t_{2g} orbital choice. Notwithstanding the small energy scale (≈ 10 K) of the system, we are able to obtain accurate results from our DFT calculations. Additionally, we observe a surprisingly large spin-lattice coupling with respect to the crystal water related degrees of freedom, which in turn manifests itself by playing an important role in determining the ground state of the system. This feature is clearly elucidated by calculating the Wannier functions, which show the effects of hydrogen bonding to the corresponding t_{2g} orbital which is oriented in the same plane as the crystal water molecule. Using the experimental position for hydrogen, we obtain a frustration ratio $\alpha \approx 1.0$ and a value of $\alpha \approx 1.4$ upon relaxing the hydrogen position in the crystal lattice. Both these values are larger than the experimental value $\alpha_{\rm exp} = 0.29$. In order to understand the origin of this discrepancy between the experiment and our calculations, we simulated the temperature dependence of the susceptibility using both the small and large values of α. Due to an intrinsic symmetry of the $J_1 - J_2$ frustrated chain model, we show that both values of α provide equally good fits to the experimental curve. Consequently, we calculated magnetization curves as a means to unambiguously distinguish the two solutions and show two features which can be used to identify the appropriate α that defines the magnetic ground state of $KTi(SO_4)_2{\cdot}H_2O$. Hence, we suggest performing high-field magnetization measurements on this system and as well as a.c. susceptibility experiments (to obtain the size of the spin-gap) at very low temperatures.

---

* Deepa.Kasinathan@cpfs.mpg.de
† rosner@cpfs.mpg.de

[1] W. E. A. Lorenz, R. O. Kuzian, S.-L. Drechsler, W.-D. Stein, N. Wizent, G. Behr, J. Málek, U. Nitzsche, H. Rosner, A. Hiess, W. Schmidt, R. Klingeler, M. Loewenhaupt, and B. Büchner, Europhys. Lett. **88**, 37002 (2009).

[2] U. Nitzsche, S.-L. Drechsler and H. Rosner, to be published.

[3] A. A. Gippius, E. N. Morozova, A. S. Moskvin, A. V. Zalessky, A. A. Bush, M. Baenitz, H. Rosner, and S.-L. Drechsler, Phys. Rev. B **70**, 020406 (2004).

[4] S.-L. Drechsler, J. Málek, J. Richter, A. S. Moskvin, A. A. Gippius, H. Rosner, Phys. Rev. Lett. **94**, 039705 (2005).

[5] M. Enderle, C. Mukherjee, B. Fak, R. Kremer, J. Broto, H. Rosner, S.-L. Drechsler, J. Richter, J. Málek, A. Prokofiev, et al., Europhys. Lett. **70**, 237 (2005).

[6] T. Masuda, A. Zheludev, A. Bush, M. Markina, and A. Vasiliev, Phys. Rev. Lett. **92**, 177201 (2004).

[7] L. Capogna, M. Mayr, P. Horsch, M. Raichle, R. Kremer, M. Sonin, and B. Keimer, Phys. Rev. B **71**, 140402 (2005).

[8] S.-L. Drechsler, J. Richter, A. Gippius, A. Vasiliev, A. Bush, A. Moskvin, Y. Prots, W. Schnelle, and H. Rosner, Europhys. Lett. **73**, 83 (2006).

[9] V. V. Mazurenko, S. L. Skornyakov, A. V. Kozhevnikov, F. Mila, and V. I. Anisimov, Phys. Rev. B **75**, 224404 (2007).

[10] J. Riera, and A. Dobry, Phys. Rev. B **51**, 16098 (1995).

[11] M. Hase, I. Terasaki, and K. Uchinokura, Phys. Rev. Lett. **70**, 3651 (1993).

[12] G. Khaliullin, and S. Maekawa, Phys. Rev. Lett. **85**, 3950 (2000).

[13] T. Kiyama, H. Saitoh, M. Itoh, K. Kodama, H. Ichikawa, J. Akimitsu, J. Phys. Soc. Jpn. **74**, 1123 (2005).

[14] A. Seidel, C. A. Marianetti, F. C. Chou, G. Ceder, and P. A. Lee, Phys. Rev. B **67**, 020405(R) (2003).

[15] G. J. Nilsen, H. M. Rønnow, A. M. Läuchli, F. P. A. Fabbiani, J. Sanchez-Benitez, K. V. Kamenev, and A. Harrison, Chem. Mater. **20**, 8 (2008).

[16] R. Jullien, and F. D. M. Haldane, Bull. Am. Phys. Soc. **28**, 344 (1983).

[17] K. Okamoto, and K. Nomura, Phys. Lett. A **169**, 433 (1992).

[18] S. Eggert, Phys. Rev. B **54**, R9612 (1996).

[19] C. K. Majumdar, and D. K. Ghosh, J. Math. Phys. **10**, 1388 (1969).

[20] C. K. Majumdar, and D. K. Ghosh, J. Math. Phys. **10**, 1399 (1969).

[21] F. D. M. Haldane, Phys. Rev. B **25**, 4925 (1982).

[22] S. R. White and I. Affleck, Phys. Rev. B **54**, 9862 (1996)

[23] E. J. Graeber, B. Morosin, and A. Rosenzweig, American Mineralogist **50**, 1929 (1965).

[24] Note that, the orbital angular momentum remains unquenched in the 2T ground state term, transforming as $-\mathbf{L}$ for $L = 1$. Spin-orbit coupling results in a pair of nonmagnetic Kramers doublets in the effective $J = 3/2$ ground state and a magnetic Kramers doublet excited state. However, the spin-orbit coupling fir Ti is rather small compared to the ligand field split due to the small distortion of the TiO_6 octahedra. Thus, we do not include the spin-orbit coupling in our calculations.

[25] T. Saha-Dasgupta, R. Valenti, H. Rosner, and C. Gros, Europhys. Lett. **67**, 63 (2004).

[26] K. Koepernik, and H. Eschrig, Phys. Rev. B **59**, 1743 (1999).
[27] I. Opahle, K. Koepernik, and H. Eschrig, Phys. Rev. B **60**, 14035 (1999).
[28] J. P. Perdew, and Y. Wang, Phys. Rev. B **45**, 13244 (1992).
[29] H. Eschrig, and K. Koepernik, Phys. Rev. B **80**, 104503 (2009).
[30] A. F. Albuquerque, F. Alet, P. Corboz, P. Dayal, A. Feiguin, S. Fuchs, L. Gamper, E. Gull, S. Gürtler, A. Honecker, R. Igarashi, M. Körner, A. Kozhevnikov, A. Läuchli, S. R. Manmana, M. Matsumoto, I. P. McCulloch, F. Michel, R. M. Noack, G. Pawlowski, L. Pollet, T. Pruschke, U. Schollwöck, S. Todo, S. Trebst, M. Troyer, P. Werner, and S. Wessel, J. Magn. Magn. Mater. **310**, 1187 (2007).
[31] X. Wang, and T. Xiang, Phys. Rev. B **56**, 5061 (1997).
[32] D. Kasinathan, K. Koepernik, and H. Rosner, Phys. Rev. Lett. **100**, 237202 (2008).
[33] The effective onsite exchange $J_{\rm d}$ has been set to 1 eV.
[34] T. Mizokawa, and A. Fujimore, Phys. Rev. B **54**, 5368 (1996). One should note that the value of U_d is depending on the basis set, the choice of the double counting scheme, etc. Thus, $U_d = 4$ eV should be considered as an approximation, only.
[35] M. Schmitt, O. Janson, M. Schmidt, S. Hoffmann, W. Schnelle, S.-L. Drechsler, and H. Rosner, Phys. Rev. B **79**, 245119 (2009).
[36] O. Janson, J. Richter, and H. Rosner, Phys. Rev. Lett. **101**, 106403 (2008).
[37] V. Szalay, L. Kovács, M. Wöhlecke, and E. Libowitzky, Chem. Phys. Lett. **354**, 56 (2002).
[38] The electron density of hydrogen, the lightest atom with only one electron is generally localized away from the nucleus and hence it is difficult to detect the exact position of the H nucleus from X-ray diffraction measurements. The relatively high electron density between the oxygen and hydrogen atoms, makes the O-H bonds to appear too short.
[39] A. Bühler, U. Löw, and G. Uhrig, Phys. Rev. B **64**, 024428 (2001).
[40] K. Okamoto, and N. Nomura, Phys. Lett. A **169**, 433 (1992).
[41] S. R. White, and I. Affleck, Phys. Rev. B. **54**, 9862 (1992).
[42] R. Nath, A. A. Tsirlin, C. Geibel, and H. Rosner, Phys. Rev. B **78**, 064422 (2008).
[43] S. Lebernegg, A. A. Tsirlin, O. Janson, R. Nath, J. Sichelschmidt, Yu. Skourski, G. Amthauer, and H. Rosner, Phys. Rev. B **84**, 174436 (2011).